Supporting Information for

Influence of Spin State and Electron Configuration on the Active Site and Mechanism for Catalytic Hydrogenation on Metal Cation Catalysts Supported on NU-1000: Insights from Experiments and Microkinetic Modeling

Hafeera Shabbir [a], Steven Pellizzeri[b], Magali Ferrandon[c], In Soo Kim[d,e], Nicolaas A. Vermeulen[f], Omar K. Farha[f,*], Massimiliano Delferro[c,*], Alex B.F. Martinson[d,*], Rachel B. Getman[a,*]

[a] Chemical and Biomolecular Engineering, Clemson University, Clemson, SC 29634, USA.

[b] Department of Chemistry and Biochemistry, Eastern Illinois University, Charleston, IL 61920, USA.

[c] Chemical Sciences and Engineering Division, Argonne National Lab, Argonne, IL 60439, USA.

[d] Materials Science Division, Argonne National Lab, Argonne, IL 60439, USA.

[e] Present address: Nanophotonics Research Center, Korea Institute of Science and Technology, Seoul 02792, South Korea.

**corresponding authors*

Contents:

Section S1:

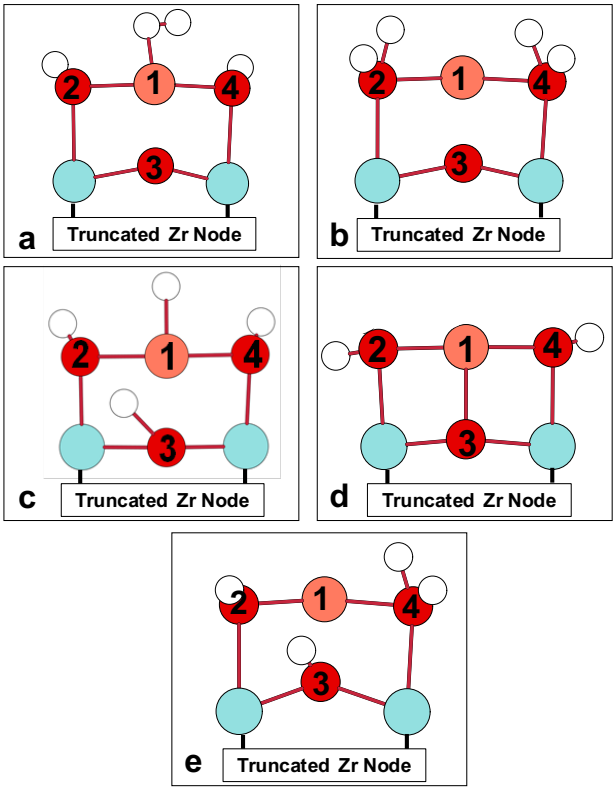

Figure S1. Proton arrangements of H atoms considered in this work. Color key: C = gray, O = red, H = white, Zr = teal, M = orange. Atoms labeled 1, 2, 3, and 4 represent the different sites where hydrogen species are allowed to bind.

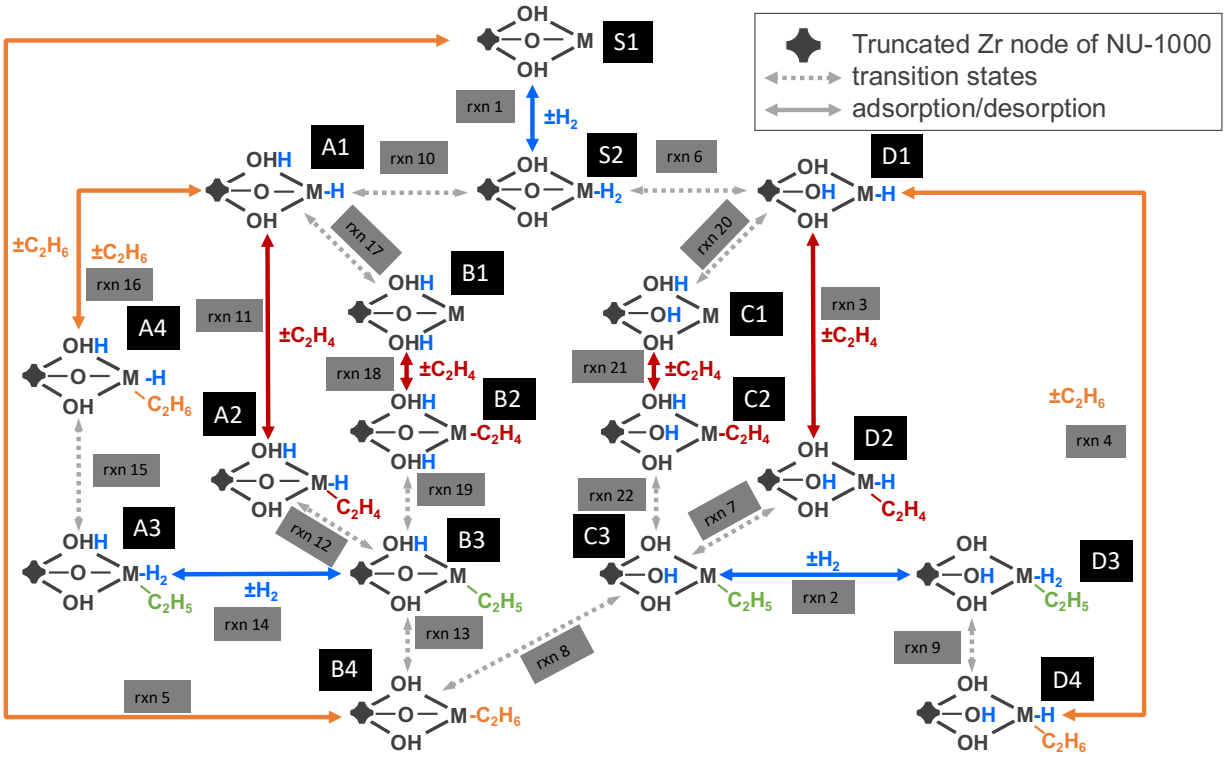

Figure S2. This is the complete reaction network explored in this work. Th reaction intermediates are denoted by an alphabet-number like S1, D2 etc. The five proton arrangements in fig S1 correspond to a= S2, b=C1, 1c=D1, d=S1 and e=A1. The solid arrows indicate adsorption/desorption of H_2, C_2H_4 and C_2H_6 and the dashed lines correspond to the activated bond formation/cleavage H-H and C-H reactions.

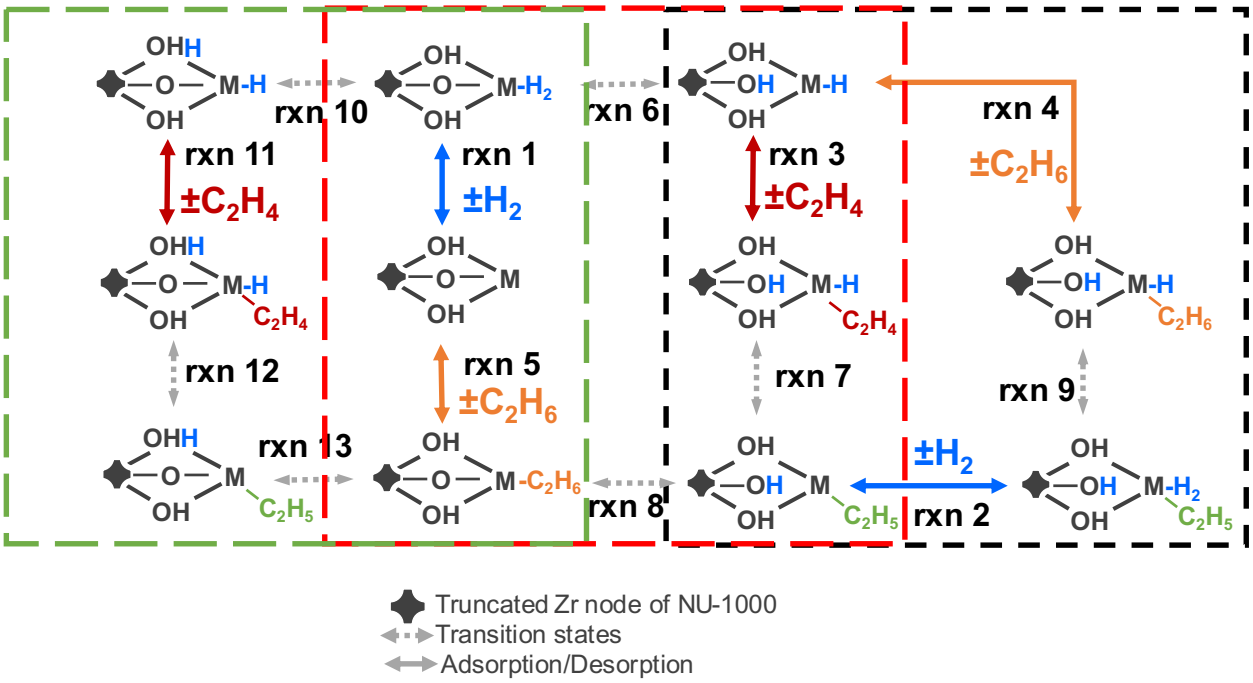

Figure S3. Dominant reaction mechanisms determined by the microkinetic model. This reaction network is a subset of the reaction network in Figure S2. The mechanism indicated by dashed black line is the SW mechanism (rxn3,7,2,9and 4) followed by Ni^{2+}, Cu^{2+} (50°C <T<150°C) and Zn^{2+}. The red dashed encompass the alternate mechanism (rxn 1,6,3,7,8 and 5) followed by high spin Mn^{2+}, $Fe^{2+}$and Co^{2+}. The green dashed line outlines the mechanism (rxn 1,10,11,12,13,5) followed by Cu^{2+} at T>150°C

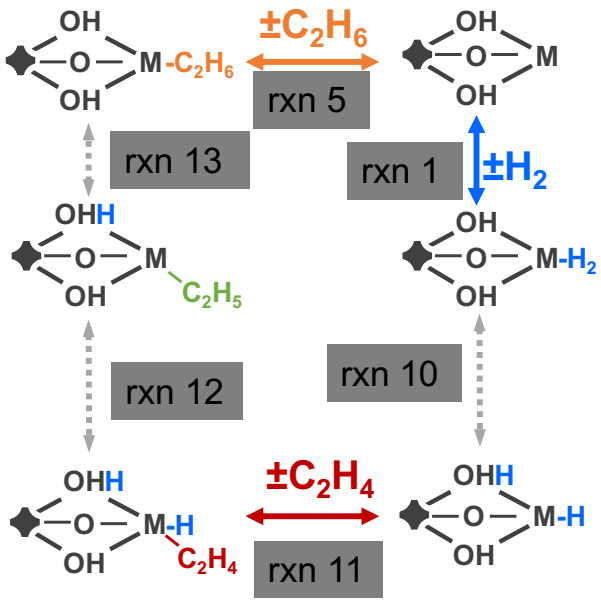

Figure S4. Reaction mechanism followed by Cu^{2+} at T>150°C

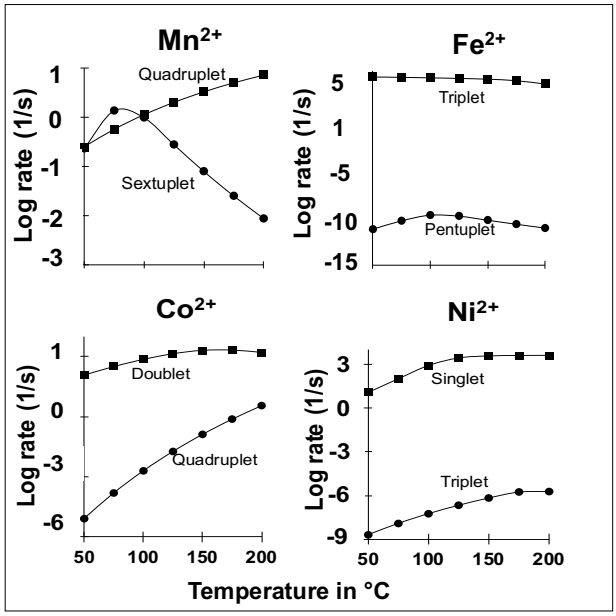

Figure S5. Theoretical rate of different multiplicities of the M-NU-1000 supported catalysts where M= Mn, Fe, Co and Ni.

Section S2:

NU-1000 Synthesis. NU-1000 was synthesized according to the procedure reported previously[1]. Briefly, $ZrOCl_2 \cdot 8H_2O$ (97 mg, 0.30 mmol) and benzoic acid (2.70 g, 22 mmol) were mixed in 8 mL of DMF (in a 6-dram vial) and dissolved using sonication. The clear solution was incubated in an oven at 80 ˚C for 1 h. After cooling down to room temperature, H_4TBAPy (40 mg, 0.06 mmol) was added to this solution and the mixture was sonicated for 10 mins. The yellow suspension was heated in an oven at 100 ˚C for 18 h. After cooling down to room temperature, yellow NU-1000 precipitate was collected by centrifuge (7800 rpm, 5 mins) and washed with fresh DMF for two times. As synthesized NU-1000 was then suspended in 13 mL of DMF and 0.5 mL of 8M HCl was added to acid-activate the zirconium node. This mixture was heated in an oven at 100 ˚C for 24 h. After cooling down to room temperature, the supernatant was removed by centrifuge, and the material was washed twice with fresh DMF. Subsequently the solid materials were washed twice with acetone and soaked in acetone for additional 12 h. Then the acetone was removed by centrifuge, and the solid was briefly dried in an oven at 80 °C. The solid material was activated on a SmartVacPrep station (Micromeritics) under dynamic vacuum at 120 ˚C until an outgassing rate of ≤ 0.002 mm Hg min^{-1} was reached.

Post-Modification of NU-1000 (AIM). NU-1000 was modified according to atomic layer deposition (**A**LD) **i**n **M**OF (**AIM**) procedures reported previously[2]. All AIM processes were performed in a commercial reactor (Savannah S200, Ultratech) with an in-line Entegris Ni filtered nitrogen (N_2). N_2 was introduced continuously into the sample chamber at a flow rate of 5 – 10 sccm to maintain a base pressure of ~0.2 Torr. The sample chamber was held at 115 °C, whereas precursor cylinders were held at various temperatures depending on the volatility of organometallic precursors (see Table S1). For saturation studies (to test self-limiting behavior), a custom-made powder sample holder containing 10 mg of NU-1000 was loaded into the sample chamber, which was left to equilibrate for 30 minutes to remove physisorbed water. The ALD reaction was performed in a quasi-static mode with a standard pulse sequence of t_1-t_2-t_3, where t_1 is the precursor pulse time, t_2 the exposure time, and t_3 the N_2 purge time (see Table S1). After the

introduction of saturating organometallic precursor, the sample was purged for 30 minutes to ensure complete removal of excess precursor in the pores of NU-1000. Finally, the sample was subjected to micropulses of H_2O (0.1 s per pulse) to minimize any heating effects.

Table S1. Vapor phase post-modification conditions for various ALD precursors.

ALD Precursor	**Precursor Temp. (°C)**	**t_1 (s)**	**t_2 (s)**	**t_3 (s)**
$ZnEt_2$	room temp.	0.1	44.9	30
FeAMD	120	0.5	89.5	60
NiAMD	120	1.5	300	300
$Cu(dmap)_2$	100	0.5	59.5	60
$Mn(EtCp)_2$	100	0.050	29.925	60
$CoCp(CO)_2$	room temp.	0.75	59.25	60

Safety and Hazards. Diethylzinc reacts violently with water and easily ignites upon contact with air. It should therefore be handled using inert atmosphere techniques. Several of the other ALD precursors are also air sensitive and will react in ambient.

Section S3:

Table S2. Gibbs free energy change in kJ/mol of reaction steps and transition barriers. The reaction numbers correspond to Figure S2. '*' represents the reaction energies that are unlikely to be part of the dominant reaction mechanism due to their high Gibbs free enegies. Numbers in parenthesis next to metals represent their multiplicity. Bold numbers represent transition barrier for that reaction

Rxn no	**Rxn Equation**	**Mn (6)**	**Mn (4)**	**Fe (5)**	**Fe (3)**	**Co (4)**	**Co (2)**	**Ni (3)**	**Ni (1)**	**Cu (2)**	**Zn (1)**
1	$M_{site1} + O_{site3} + H\text{-}O_{site2/4} + H_2\,(g) \leftrightarrow H_2\text{-}M_{site1} + O_{site3} + H\text{-}O_{site2/4}$	-13	-17	-9	-44	-3	-30	9	-28	6	7
2	$C_2H_5 - M_{site1} + H{-}O_{site1/2/3} + H_2\,(g) \leftrightarrow (H_2/C_2H_5) - M_{site1} + H{-}O_{site1/2/3}$	46	42	4	-9	47	-21	17	31	22	21
3	$H\text{-}M_{site1} + H\text{-}O_{site1/2/3} + C_2H_4\,(g) \leftrightarrow (H/C_2H_4\text{-}M_{site1}) + H\text{-}O_{site1/2/3}$	3	-80	-30	-47	-8	-95	-7	-106	26	20
4	$H\text{-}M_{site1} + H\text{-}O_{site1/2/3} + C_2H_6\,(g) \leftrightarrow (H/C_2H_6\text{-}M_{site1}) + H\text{-}O_{site1/2/3}$	40	43	53	50	20	-20	14	4-9	25	15
5	$M_{site1} + H_2\text{-}O_{site2/4} + O_{site3} + C_2H_6\,(g) \leftrightarrow C_2H_6\text{-}M_{site1} + H_2\text{-}O_{site2/4} + O_{site3}$	-28	38	8	11	-14	9	6	33	21	-1
6	$H_2\text{-}M_{site1} + H\text{-}O_{site2/4} + O_{site3} \leftrightarrow H\text{-}M_{site1} + H\text{-}O_{site\ 2/3/4}$	-7 **68**	-12 **90**	-11 **74**	3 **109**	-61 **30**	1 **118**	-32 **61**	-30 **70**	-84 **69**	-85 **58**

7	$(H/C_2H_4)\text{-}M_{site1} + H\text{-}O_{site2/3/4} \leftrightarrow C_2H_5\text{-}M_{site1} + H\text{-}O_{site2/3/4}$	-69 **77**	-2 **40**	-15 **80**	2 **13**	-71 **44**	10 **29**	-68 **15**	-43 **18**	-114 **12**	-86 **91**
8	$C_2H_5\text{-}M_{site1} + H\text{-}O_{site1/2/3} \leftrightarrow C_2H_6\text{-}M_{site1} + H\text{-}O_{site2/4}$	-75 **85**	16 **98**	-60 **93**	-36 **102**	-2 **110**	-9 **133**	-29 **115**	108 **234**	53 **149**	22 **141**
9	$(H_2/C_2H_5)\text{-}M_{site1} + H\text{-}O_{site1/2/3} \leftrightarrow (H/C_2H_6)\text{-}M_{site1} + H\text{-}O_{site1/2/3}$	-73 **47**	-49 **27**	-39 **67**	-28 **36**	-79 **76**	-46 **38**	-60 **101**	-63 **17**	-42 **75**	-72 **143**
10	$H_2\text{-}M_{site1} + H\text{-}O_{site2/4} + O_{site3} \leftrightarrow H\text{-}M_{site1} + H_2\text{-}O_{site\ 2} + O_{site\ 3} + H\text{-}O_{site\ 4}$	37 **74**	70 **100**	51 **81**	82 **112**	1 **43**	62 **90**	13 **209**	33 **95**	-10 **58**	-47 **54**
11	$H\text{-}M_{site1} + H_2\text{-}O_{site2} + O_{site3} + H\text{-}O_{site4} + C_2H_4\,(g) \leftrightarrow (H/C_2H_4)\text{-}M_{site1} + H_2\text{-}O_{site2} + O_{site3} + H\text{-}O_{site4}$	34	-148	15	-113	40	-105	27	-114	5	18
12	$(H/C_2H_4)\text{-}M_{site1} + H\text{-}O_{site2} + O_{site3} + H_2\text{-}O_{site4} \leftrightarrow C_2H_5\text{-}M_{site1} + H\text{-}O_{site2} + O_{site3} + H_2\text{-}O_{site4}$	-103 **49**	18 *****	-101 **29**	-16 **22**	-119 **19**	3 **40**	-98 **15**	-41 **19**	-111 *****	-95 **131**
13	$C_2H_5\text{-}M_{site1} + H\text{-}O_{site2} + O_{site3} + H_2\text{-}O_{site4} \leftrightarrow C_2H_6\text{-}M_{site1} + H\text{-}O_{site2/4} + O_{site3}$	-116 **41**	-18 **122**	-81 **55**	-31 **93**	-65 **56**	-54 **69**	-79 **61**	52 **160**	-2 **103**	-17 **101**
14	$C_2H_5\text{-}M_{site1} + H\text{-}O_{site2} + O_{site3} + H_2\text{-}O_{site4} + H_2\,(g) \leftrightarrow (H_2/C_2H_5)\text{-}M_{site1} + H\text{-}O_{site2} + O_{site3} + H_2\text{-}O_{site4}$	18	18	24	32	21	-9	26	45	31	37
15	$(H_2/C_2H_5)\text{-}M_{site1} + H\text{-}O_{site2} + O_{site3} + H_2\text{-}O_{site4} \leftrightarrow (H/C_2H_6)\text{-}M_{site1} + H\text{-}O_{site2} + O_{site3} + H_2\text{-}O_{site4}$	-54 **97**	-1 **26**	-22 **103**	-24 **31**	-46 **86**	-30 **13**	-59 **76**	-33 **16**	-43 **66**	-64 **171**

16	$H\text{-}M_{site1} + H_2\text{-}O_{site2} + O_{site3} + H\text{-}O_{site4} + C_2H_6\,(g) \leftrightarrow (H/C_2H_6)\text{-}M_{site1} + H_2\text{-}O_{site2} + O_{site3} + H\text{-}O_{site4}$	27	19	49	11	28	-8	29	11	14	28
17	$M_{site1} + H_2\text{-}O_{site\ 2/4} + O_{site\ 3} \leftrightarrow H\text{-}M_{site1} + H_2\text{-}O_{site\ 2} + O_{site\ 3} + H\text{-}O_{site\ 4}$	271 *	117 *	226 *	144 *	* *	127 *	188 *	119 *	* *	142 *
18	$M_{site1} + H_2\text{-}O_{site2/4} + O_{site3} + C_2H_4\,(g) \leftrightarrow C_2H_4\text{-}M_{site1} + H_2\text{-}O_{site2/4} + O_{site3}$	-47	-120	-51	-184	R	-155	-255	-202	*	35
19	$C_2H_4\text{-}M_{site1} + H_2\text{-}O_{site2/4} + O_{site3} \leftrightarrow C_2H_5\text{-}M_{site1} + H\text{-}O_{site2} + O_{site3} + H_2\text{-}O_{site4}$	-292 **2**	-128 **0**	-260 **0**	-88 **37**	-224 *	-74 **24**	-3 **191**	-72 **47**	-137 **1**	-254 **46**
20	$H\text{-}M_{site1} + H\text{-}O_{site\ 2/3/4} \leftrightarrow M_{site1}+H_2\text{-}O_{site\ 2} + H\text{-}O_{site\ 3/4}$	256 *	236 *	236 *	167 *	* *	162 *	176 *	132 *	* *	150 *
21	$M_{site1} + H_2\text{-}O_{site2} + H\text{-}O_{site3/4} + C_2H_4\,(g) \leftrightarrow C_2H_4\text{-}M_{site1} + H_2\text{-}O_{site2} + H\text{-}O_{site3/4}$	-42	-240	-66	-179	*	-181	-70	-211	*	-149
22	$C_2H_4\text{-}M_{site1}+H_2\text{-}O_{site\ 2} + H\text{-}O_{site\ 3/4} \leftrightarrow (C_2H_5)\text{-}M_{site1}+H\text{-}O_{site\ 2/3/4}$	-279 **0**	-77 **65**	-216 **0**	-33 **87**	-220 **3**	-67 **33**	-181 **0**	-70 **50**	-142 **0**	-67 **223**

Table S3. Gibbs free energy in kJ/mol of all reaction intermediates (refer to fig S2 for nomenclature) at T=273.15 K and P=1atm. Numbers in parenthesis next to metals represent their multiplicity/spin state. '*' represents the reaction intermediates that are unlikely to be part of the dominant reaction mechanism due to their high Gibbs free energies.

No	Mn (6)	Mn (4)	Fe (5)	Fe (3)	Co (4)	Co (2)	Ni (3)	Ni (1)	Cu (2)	Zn (1)
S1	-4158.531933	-4158.468448	-4271.216973	-4271.163844	-4390.250698	-4390.227623	-4515.800216	-4515.764896	-4647.948236	-4786.842908
S2	-4159.705521	-4159.64343	-4272.388996	-4272.349143	-4391.420692	-4391.407674	-4516.965431	-4516.944	-4649.114533	-4788.008891
A1	-4159.691248	-4159.61665	-4272.369721	-4272.318079	-4391.420229	-4391.38412	-4516.960342	-4516.932	-4649.11852	-4788.02668
A2	-4238.161982	-4238.156945	-4350.847677	-4350.845102	-4469.88873	-4469.907953	-4595.433738	-4595.459	-4727.600292	-4866.503591
A3	-4239.363301	-4239.312019	-4352.045613	-4352.007544	-4471.094989	-4471.078701	-4596.629651	-4596.626	-4728.799489	-4867.694251
A4	-4239.383896	-4239.312296	-4352.054027	-4352.016664	-4471.112586	-4471.090043	-4596.65219	-4596.639	-4728.816041	-4867.718813
B1	-4159.588051	-4159.572027	-4272.283659	-4272.263336	*	-4391.335844	-4516.888821	-4516.886	*	-4787.97248
B2	-4238.089945	-4238.1014	-4350.787045	-4350.81743	-4469.848932	-4469.878528	-4595.469943	-4595.447	-4727.590364	-4866.442972
B3	-4238.201299	-4238.150061	-4350.886162	-4350.851007	-4469.934184	-4469.906659	-4595.470899	-4595.475	-4727.642546	-4866.53973
B4	-4238.245537	-4238.156945	-4350.91701	-4350.862679	-4469.958837	-4469.927044	-4595.501	-4595.455	-4727.643252	-4866.546112
C1	-4159.610543	-4159.558338	-4272.303206	-4272.284387	*	-4391.34547	-4516.910423	-4516.905	*	-4787.988554
C2	-4238.110339	-4238.133529	-4350.812133	-4350.836339	-4469.874123	-4469.898174	-4595.420966	-4595.47	-4727.609488	-4866.52897
C3	-4238.216791	-4238.163048	-4350.894253	-4350.849085	-4469.957895	-4469.923674	-4595.489849	-4595.496	-4727.663526	-4866.554646
D1	-4159.708063	-4159.648155	-4272.393269	-4272.347897	-4391.44388	-4391.407351	-4516.977484	-4516.956	-4649.146411	-4788.045584
D2	-4238.190631	-4238.162429	-4350.888643	-4350.849651	-4469.930711	-4469.927462	-4595.4641	-4595.48	-4727.620285	-4866.521967
D3	-4239.367947	-4239.315871	-4352.061244	-4352.021322	-4471.108817	-4471.100312	-4596.65218	-4596.653	-4728.823735	-4867.715401
D4	-4239.395871	-4239.334544	-4352.076012	-4352.031863	-4471.139054	-4471.117878	-4596.674915	-4596.677	-4728.839799	-4867.742656

Table S4. Gibbs free energy in kJ/mol of all transition state structures (refer to fig S2 for nomenclature) at T=273.15 K and P=1atm. '*' represents the reaction intermediates that are unlikely to be part of the dominant reaction mechanism due to their high Gibbs free energies. Numbers in parenthesis next to metals represent their multiplicity.

TS	Mn (6)	Mn (4)	Fe (5)	Fe (3)	Co (4)	Co (2)	Ni (3)	Ni (1)	Cu (2)	Zn (1)
S2-A1	-4159.677479	-4159.605492	-4272.357978	-4272.306605	-4391.4044	-4391.373305	-4516.885759	-4516.908	-4649.092607	-4787.992471
S2-D1	-4159.679479	-4159.608956	-4272.254574	-4272.307521	-4391.409248	-4391.362875	-4516.94201	-4516.917657	-4649.088335	-4787.991191
A1-B1	*	*	*	*	*	*	*	*	*	*
D1-C1	*	*	*	*	*	*	*	*	*	*
A2-B3	-4238.14348	*	-4350.836787	-4350.836892	-4469.881595	-4469.892858	-4595.427954	-4595.451845	-4727.600958	-4866.453694
A3-A4	-4239.326382	-4239.302016	-4352.006327	-4351.995923	-4471.062249	-4471.073592	-4596.600543	-4596.620146	-4728.774217	-4867.629172
B2-B3	-4238.089066	-4238.10928	-4350.794591	-4350.803218	*	-4469.869529	-4595.397269	-4595.429	-4727.590137	-4866.425572
B3-B4	-4238.1857	-4238.103458	-4350.865285	-4350.815673	-4469.912701	-4469.880409	-4595.447705	-4595.414	-4727.603211	-4866.501132
C3-B4	-4238.184378	-4238.125682	-4350.858728	-4350.810363	-4469.916127	-4469.872885	-4595.446175	-4595.407	-4727.606756	-4866.500954
C2-C3	-4238.116699	-4238.108581	-4350.813849	-4350.803172	-4469.872806	-4469.885414	*	-4595.451	-4727.609872	-4866.444045
D2-C3	-4238.161231	-4238.147254	-4350.858309	-4350.844737	-4469.914071	-4469.916309	-4595.458574	-4595.473	-4727.615816	-4866.487209
D3-D4	-4239.350108	-4239.305627	-4352.035841	-4352.00723	-4471.08004	-4471.085699	-4596.613618	-4596.647	-4728.795292	-4867.660866

Table S5. Experimental conversion of ethene under reaction conditions for the metals and NU-1000 support. All values are in percentage, 1st pass designates the first ten minute run and 2nd pass the next ten minute run on the high throughput reactor

Metal	**Cu**		**Co**		**Fe**		**Mn**		**Ni**		**Zn**		**NU-1000**	
Temperature	1st pass	2nd pass	1st pass	2nd pass	1st pass	2nd pass	1st pass	2nd pass	1st pass	2nd pass	1st pass	2nd pass	1st pass	2nd pass
50	1.07	0.94	5.19	6.80	0.67	0.09	0.67	0.12	1.35	60.52	0.59	0.09	0.58	0.08
75	1.58	2.52	9.36	10.49	0.48	0.11	0.67	0.45	2.77	77.52	0.38	0.09	0.34	0.08
100	2.36	4.63	14.19	13.27	0.41	0.21	1.46	1.21	4.81	83.53	0.27	0.13	0.18	0.09
125	2.87	5.90	13.52	12.95	0.41	0.34	1.70	1.52	5.32	82.36	0.31	0.25	0.12	0.09
150	2.57	4.09	8.93	7.98	0.41	0.39	1.75	1.63	4.93	73.29	0.33	0.31	0.11	0.11
175	3.35	4.50	5.11	4.86	0.42	0.38	1.48	1.41	4.34	68.95	0.33	0.32	0.09	0.10
200	3.70	4.70	2.34	2.52	0.39	0.36	1.44	1.11	30.90	81.06	0.27	0.28	0.11	0.11

Table S6. Mulliken Spin orbital populations and metal hydrogen bond distances (refer to Figure S2 for nomenclature)

Metal-Multiplicity-Structure	Total *d* orbital population	Alpha *d* orbital population	Beta *d* orbital population	Spin *d* orbital population	Metal-Hydrogen bond distance in Angstrom
Mn-sextet-S2	5.46202	5.0004	0.46161	4.53879	2.0874
Mn-sextet-D3	5.48739	5.03876	0.4486	4.59016	2.4982
Fe-quintet-S2	6.41143	4.98622	1.42521	3.56102	1.7343
Fe-quintet-D3	6.47744	5.00257	1.47488	3.52769	1.8448
Co-quartet-S2	7.42013	4.98382	2.43632	2.54754	1.7558
Co-quartet-D3	7.55832	4.99387	2.56445	2.4294	1.8015

Section S4:

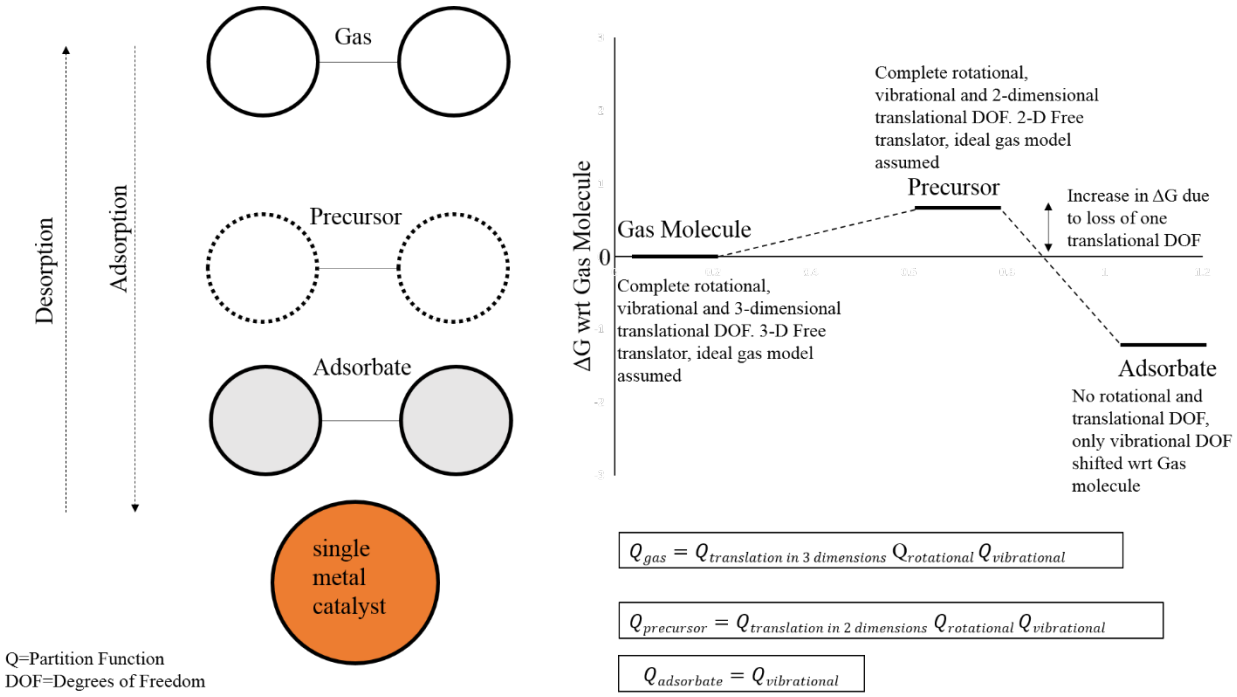

Figure S6. Assumptions in derivations of adsorbtion and desorption rate constants for construction of Gas, precursor and adsorbate partition functions

1. Assumptions:

To model the adsorption/desorption process as shown schematically in figure S6 we assume that[3,4]

1. Gas phase molecules are ideal.
2. Adsorption and desorption proceed through a "mobile precursor" which possesses two translational degrees of freedom and full rotational and vibrational degrees of freedom.
3. Translational, rotational, and vibrational partition functions for gas molecules are calculated using the particle in a box/particle on a plane, rigid rotor, and harmonic oscillator models, respectively.
4. Thermal effects due to vibration upon adsorption/desorption are assumed to be negligible with respect to thermal effects due to translation and rotation; hence the ratio of vibrational partition functions between the mobile precursor and the gas molecule is~ 1.
5. Transition state theory (TST) can be used to model the kinetics of adsorption and desorption.

2. Derivation of rate constants of adsorption and desorbtion:

Adsorption Rate Constant

For adsorption reaction, using the Transition State Theory (TST)[4], the rate constant is given by

$$k_{adsorption} = \text{rate constant of adsorption} = \frac{k_b T}{h}\ exp^{\frac{-(G_{precursor} - G_{gas})}{k_b T}}$$

The relation between the Gibbs free energy (G), entropy (S), enthalpy (H) and partition function (Q) is[5],

$$G = H - TS$$

$$S = k_b ln\ Q$$

$$G_{precursor} - G_{gas} = H_{precursor} - H_{gas} - k_b T(\ln Q_{precursor} - \ln Q_{gas})$$

$$k_{adsorption} = \frac{k_b T}{h}\ exp^{-(\frac{H_{precursor} - H_{gas} - k_b T(\ln Q_{precursor} - \ln Q_{gas})}{k_b T})}$$

$$k_{adsorption} = \frac{k_b T}{h}\frac{Q_{precursor}}{PF_{gas}}\ exp^{-(\frac{H_{precursor} - H_{gas}}{k_b T})}$$

From the PES in Figure S6, $H_{precursor} = H_{gas}$. Hence,

$$k_{adsorption} = \frac{k_b T}{h}\frac{Q_{precursor}}{Q_{gas}}$$

Substituting partition functions for precursor and gas given in figure S6 in the equation for $k_{adsorption}$,

$$k_{adsorption} = \frac{k_b T}{h}\frac{Q_{tranlsation\ in\ 2D} Q_{rotational} Q_{vibrational}}{Q_{translation\ in\ 3D} Q_{rotational} Q_{vibrational}}$$

As the precursor has not yet adsorbed, the precursor and the gas molecule have the same rotational and vibrational partition functions. Hence,

$$k_{adsorption} = \frac{k_b T}{h}\frac{Q_{tranlsation\ in\ 2D}}{Q_{translation\ in\ 3D}}$$

The partition functions for translation in 2-D and 3-D are[6],

$$Q_{translation\ in\ 2-dimensions} = \frac{L^2(2\pi m k_b T)}{h^2}$$

$$Q_{translation\ in\ 3-dimensions} = \frac{L^3(2\pi m k_b T)^{\frac{3}{2}}}{h^3}$$

Substituting the partition functions above in the equation for $k_{adsorption}$,

$$k_{adsorption} = \frac{k_b T}{h} \frac{L^2(2\pi m k_b T)}{h^2} \frac{h^3}{L^3(2\pi m k_b T)^{\frac{3}{2}}}$$

Substituting $A=L^2$, $V=L^3$ and $P = \frac{k_b T}{V}$ (which is the ideal gas law),

$$\boxed{k_{adsorption} = \frac{PA}{(2\pi m k_b T)^{1/2}}}$$

Desorption Rate Constant

Calculating the desorption rate constant using the TST[4] assumption,

$$k_{desorption} = \text{rate constant of desorption} = \frac{k_b T}{h}\ exp^{\frac{-(G_{precursor} - G_{adsorbate})}{k_b T}}$$

The expression for G is,[5]

$$G_{precursor} - G_{adsorbate} = H_{precursor} - H_{adsorbate} - k_b T(\ln Q_{precursor} - \ln Q_{adsorbate})$$

Substituting the expression above in equation for $k_{desorption}$,

$$k_{desorption} = \frac{k_b T}{h} \frac{Q_{precursor}}{Q_{adsorbate}}\ exp^{-(\frac{H_{precursor} - H_{adsorbate}}{k_b T})}$$

Assuming $H_{precursor} - H_{adsorbate} \approx \Delta E_{desorption}$, which is the zero-point corrected potential energy of desorption,

$$k_{desorption} = \frac{k_b T}{h} \frac{Q_{precursor}}{Q_{adsorbate}}\ exp^{-(\frac{\Delta E_{desorption}}{k_b T})}$$

Substituting the Q for precursor and adorbate given in figure S6,

$$k_{desorption} = \frac{k_b T}{h} \frac{Q_{tranlsation\ in\ 2D} Q_{rotational} Q_{vibrational}}{Q_{vibrational}}$$

Assuming that thermal effects due to vibration upon adsorption/desorption are negligible with respect to thermal effects due to translation and rotation, the ratio of vibrational partition functions is ~ 1. Applying this assumption and performing further substitutions[6]:

$$Q_{rotational} = \frac{8\pi^2 I k_b T}{\sigma h^2}$$

$$Q_{tranlation\ in\ 2-dimensions} = \frac{L^2(2\pi m k b T)}{h^2}$$

$\theta = \frac{h^2}{8\pi^2 I k_b}$ is the characteristic temperature for rotation

$$k_{desorption} = \frac{k_b T^3}{h^3} \frac{A(2\pi m k_b)}{\sigma\theta} exp^{-(\frac{E_{desorption}}{k_b T})}$$

Abbreviations:

Q = Partition Function

$k_{adsorption}$= Rate constant of adsorption

$k_{desorption}$= Rate constant of desorption

G=Gibbs Free energy

H = Enthalpy

S = Entropy

k_b = Boltzmann constant

h = Planck's constant

T = Temperature

σ = symmetry number represents the number of indistinguishable orientations of the particular molecule as a result of rotation

θ = characteristic temperature for rotation

P = partial pressure of the molecule in the gas phase

V = volume occupied by gas

A = denotes the area of the surface site on which the molecule absorbs

M = molar mass of the gas

$\Delta E_{desorption}$ = zero-point corrected energy of desorption

L = Dimension of translation

I = moment of inertia about an axis perpendicular to the axisthrough the center of mass of molecule

Section S5:

Experimental: The experimental apparent energies of activation were calculated using the three lowest temperatures (50, 75, and 100 °C) during the first pass of the catalytic run for Co@NU-1000, Cu@NU-1000, Mn@NU-1000 and Ni@NU-1000. The corresponding Arrhenius plots are shown in Figure S7.

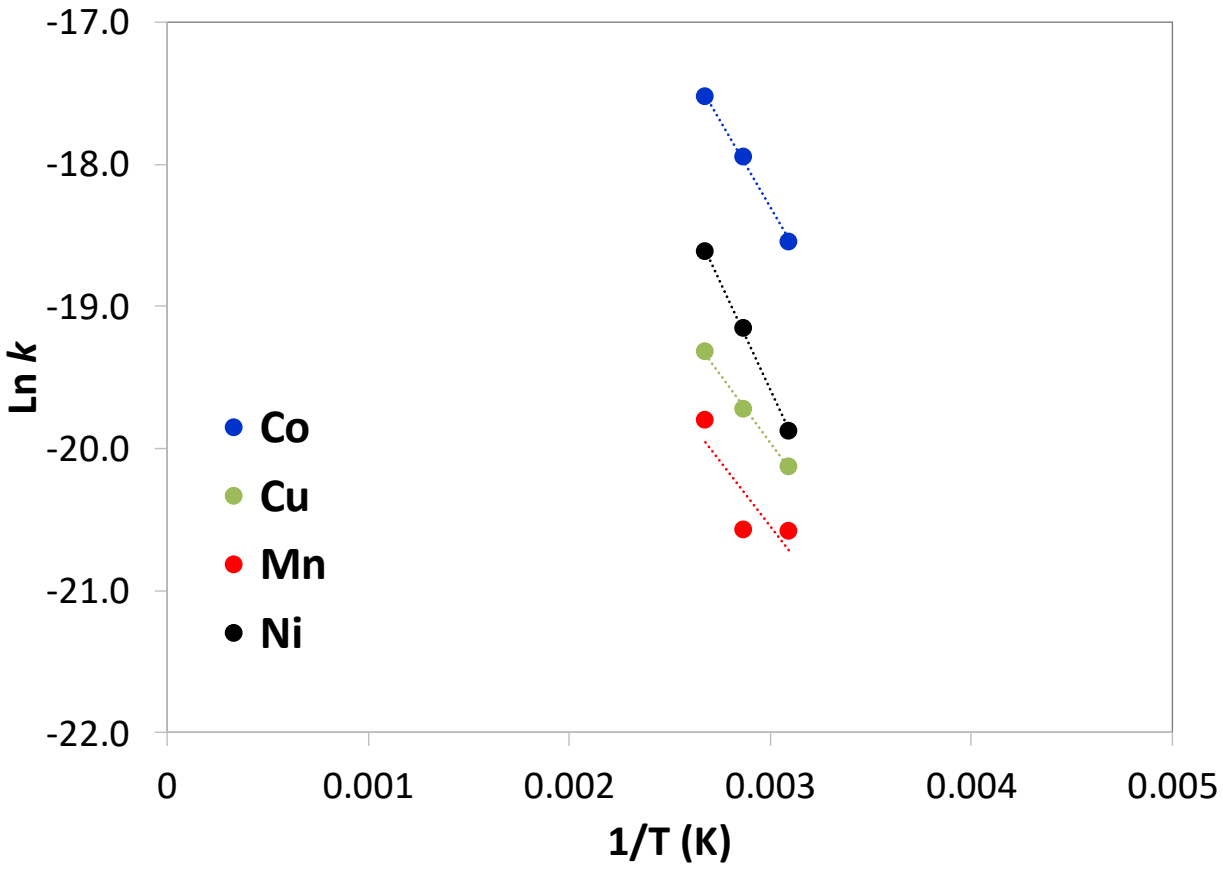

Figure S7. Arrhenius plot for Co@NU-1000, Cu@NU-1000, Mn@NU-1000 and Ni@NU-1000 for experimental rates

Theoretical: The theoretical apparent activation energies were extracted from the microkinetic model for for Co, Cu and Ni for temperatures 50, 75, and 100 °C. For Mn the values at 50 and 75 °C were considered. The values at these tempertures were chosen because the logarithm of the rate either increases or remains ~ constant with temperature. Values are provided in Table S7.

Table S7. Apparent activation energies calculated in microkinetic modeling

Theoretical variation of Eact (kJ/mol) with temperature from mkm results						
Eact(kJ/mol)						
Temperature (K)	Mn	Co	Fe	Cu	Ni	Zn
323	79.4	109.7	72.9	56.2	4.7	93.1
348	36.0	109.8	85.9	55.6	3.9	88.5
373	-52.3	109.8	100.2	55.8	3.0	63.2
398	-68.2	109.9	108.7	59.4	1.6	16.6
423	-71.8	109.9	112.4	71.9	-1.5	-4.3
448	-73.8	109.9	112.7	94.0	-8.5	-9.9
473	-75.4	109.8	96.4	111.2	-22.5	-12.3
Average of positive values	58	110	98	72	2	65

References

1 T. C. Wang, N. A. Vermeulen, I. S. Kim, A. B. F. Martinson, J. F. Stoddart, J. T. Hupp and O. K. Farha, *Nat. Protoc.,* 2016, **11**, 149-162.

2 I. S. Kim, S. Ahn, N. A. Vermeulen, T. E. Webber, L. C. Gallington, K. W. Chapman, R. L. Penn, J. T. Hupp, O. K. Farha, J. M. Notestein and A. B. F. Martinson, *J. Am. Chem. Soc.,* 2020, **142**, 242-250.

3 I. A. W. Filot, *Introduction to Microkinetic Modeling*, Technische Universiteit Eindhoven, 2018.

4 R. D. Cortright and J. A. Dumesic, *Adv. Catal.*, 2001, **46**, 161-264.

5 D. A. McQuarrie, *Statistical Mechanics*, University Science Books, Sausalito, CA, 2000.

6 D. A. McQuarrie and J. D. Simon, *Molecular Thermodynamics*, University Science Books, Sausalito, CA, 1999.